

Soft Symbol Decoding in Sweep-Spread-Carrier Underwater Acoustic Communications: A Novel Variational Bayesian Algorithm and its Analysis

Arunkumar K.P. and Chandra R. Murthy

Abstract—Sweep spread carrier (S2C) based underwater acoustic (UWA) communications is a practically attractive but less explored modulation scheme in the published literature. In this paper, we present a rigorous treatment of the S2C communication receiver design and propose a data detection scheme that can handle challenging UWA channels. State-of-the-art S2C receivers based on the gradient heterodyne processing are only effective when the path delay and Doppler spread are moderate. We develop a new variational soft symbol decoding (VSSD) algorithm based on the principle of variational Bayes’ inference for a general linear channel model. In channels with moderate delay and Doppler spreads, we show that the VSSD algorithm is equivalent to the existing gradient heterodyne receivers for S2C communications. We apply the VSSD algorithm to the i.i.d. Gaussian multiple-input multiple-output channel and show, through numerical simulations, that it far outperforms the minimum mean squared error (MMSE) data detection. We illustrate the dramatic improvement in the performance of the VSSD based S2C receiver in two different models of simulated UWA channels and two contrasting measured UWA environments publicly available in the WATERMARK channel dataset. The proposed VSSD algorithm recovers data symbols at a signal-to-noise ratio (SNR) which is at least 10 dB (8 dB) lower than the MMSE decoder for uncoded (rate 2/3 LDPC coded) communications over UWA channels where the existing receivers either fail completely or must compromise on the data rate to maintain the bit error rate (BER) performance.

Index Terms—Underwater acoustic communications, sweep spread carrier communication, variational Bayes’.

I. INTRODUCTION

Undersea exploration and monitoring presents vast opportunities and challenges alike – but a major hurdle to such missions arises from the difficulties in communicating underwater over long distances. Severe attenuation in the marine medium limits the range of electromagnetic, optical and magnetic induction based communications to just a few meters, leaving acoustic communications as the *de facto* means for wireless data transfer across tens of kilometers [2]–[4]. All the same, underwater acoustic (UWA) channels are by far the most difficult media for communication. They present a serious bottleneck in marine data networks due to limited data rate and large power demand. In particular, the data rates are limited by large delay spreads and path-dependent

Doppler shifts. Multipath propagation of sound results in a delay spread in the order of tens of milliseconds [5] and time variations cause path-dependent Doppler shifts that are non-uniform over the bandwidth of the acoustic signal. Also, the communication nodes in an underwater sensor network are usually battery operated, and are therefore highly constrained on the amount of transmission power. High performance receivers, that recover data symbols at a low signal-to-noise ratio, are highly desirable in these applications.

Sweep spread carrier (S2C) communications [6] is inspired by the chirp, whistle and song type signaling used by dolphins and whales to communicate over long distances [7]. It uses linear frequency modulated (LFM) waveforms as carriers of digital data. The S2C transmission waveform, modulated by unimodular signal constellations such as quadrature phase shift keying (QPSK), has an ideal peak-to-average power ratio (PAPR). The technique is therefore battery friendly and implemented in a wide range of full-duplex commercial acoustic modems that are used in underwater sensor networks comprising autonomous underwater vehicles (AUVs), autonomous surface vehicles (ASVs), and moored underwater sensor nodes [8]–[11]. Secure, reliable and covert communications, with a low probability of intercept, is rendered possible due to use of high bandwidth coded chirp carriers whose exact pattern is known only to the transmitter and designated receiver. The details of the S2C transmitter and receiver side processing, performance analysis, and experimental results can be found in [12]–[16]. Despite its practical merits, success with real world deployment, and commercialization, relatively few published works such as [17] have explored and developed S2C communication further. In this paper, we present a rigorous treatment of the S2C design principles, and propose an improved S2C receiver that can handle challenging UWA channels.

The S2C receiver in [6] extracts only the copy of a symbol arriving along the direct path. As a consequence, the part of the transmitted symbol energy arriving along paths other than the direct path is ignored. In [17], the authors use a maximum ratio combiner (MRC), which improves the performance of an S2C receiver by leveraging multipath diversity. The receiver in [17] performs well only when: (a) the ratio of the maximum delay spread to minimum differential delay among path arrivals is below a certain value, and (b) the Doppler spread is small. If either condition is violated, the intersymbol interference (ISI) cancellation becomes imperfect and MRC becomes suboptimal and ineffective.

The authors in [6] and [17] did not consider the effect

Arunkumar K. P. is with the Naval Physical Oceanographic Laboratory, Kochi 682 021, India (e-mail: arunkumar@npol.drdo.in). This work was carried out as part of the PhD program at Indian Institute of Science, Bangalore. Chandra R. Murthy is with the Dept. of ECE, Indian Institute of Science, Bangalore 560 012, India (e-mail: cmurthy@iisc.ac.in). A part of this work was published in [1].

of Doppler. Doppler due to relative motion between the source and receiver manifests as dilation/compression of the transmitted waveform. The effect of Doppler in underwater acoustic communications cannot be modeled as a frequency shift unless the waveform has a small time-bandwidth product. For large time-bandwidth product waveforms, typical of S2C communications, even for small relative speeds (comparable to $c/2\gamma$, where c is the speed of sound in water and γ is the time-bandwidth product of the transmitted signal), the underwater channel is best modeled as a wideband delay-scale channel [18]–[20]. In this paper, we consider an S2C communication system similar to [6] and [17] but for the more general underwater channel model that includes the time-scaling effect of Doppler on the transmitted waveform.

Previous studies on UWA communications have considered the MMSE equalizer for (hard) data symbol detection or joint channel estimation and data detection in orthogonal frequency division multiplex (OFDM) and code division multiple access (CDMA) based communications [21]–[25]. However, in coded communications, it is more important to estimate the soft symbols rather than perform hard symbol decision [26]. The variational Bayes' (VB) inference is a promising approach to obtain soft symbol estimates because, by design, it directly infers the posterior distributions of the transmitted data symbols. However, to the best of our knowledge, other than our initial work in the area [1], [27], [28], VB based soft symbol estimation has not been explored in the literature.

In this paper, we present a new mathematical framework for S2C communications. Based on this, we develop a new decoder that uses the principle of variational Bayes' inference to determine the soft symbol estimates in harsh UWA channel environments. Our specific contributions are:

- 1) We present a mathematical framework for S2C data detection in doubly-spread UWA channels.
- 2) We show that the S2C receivers in [6] and [17] closely approximate the minimum mean squared error (MMSE) decoder for the AWGN channel and moderately delay spread UWA channels with well resolved path delays.
- 3) Previous works considered benign channels, but in practice the channel is rarely benign. We theoretically analyze the limitations of the existing S2C receivers in highly spread UWA channels and elicit the need to consider better receivers such as the MMSE receiver designed for the system model in this paper.
- 4) In coded communications, it is required to obtain good soft-symbol estimates, which the previous S2C receivers do not consider. Using the VB inference approach, we derive a new iterative log-likelihood ratio (LLR) based soft symbol decoding receiver.
- 5) We show that the fixed point iterations for LLR based soft symbol decoding converge to a local optimum in the general case, and to a global optimum for orthogonal channel matrices whose important special cases are the AWGN and Rayleigh channels. Specifically, in AWGN and Rayleigh channels, we show that the proposed variational soft symbol decoder (VSSD) is a maximum-likelihood (ML) decoder and converges in a single iteration.

- 6) Through extensive numerical studies, we demonstrate the strong performance of the VSSD in harsh simulated channels where existing S2C receivers fail completely. For the WATERMARK channel dataset, we develop a suitable baseband measurement model for the S2C system and present the superior performance of the proposed decoder in two contrasting real world channels.

We develop the system model in Section II. In Section III, we derive the existing S2C receivers as specialized MMSE symbol decoders and elicit the limitations of these receivers in Section IV. In Section V, we present improved S2C receivers – the MMSE decoder and the new VSSD – that can handle harsh channel conditions. We present the results of our numerical studies in Section VI and conclude in Section VII.

II. SYSTEM MODEL

Consider an S2C system as in [6] and [17]. At the transmitter side, the carrier waveform is a succession of linear frequency modulated chirp pulses, each swept from a lower frequency limit f_L to an upper frequency limit f_H over a sweep duration T_{sw} , given by:

$$c(t) = e^{j\phi(t)}, \quad 0 \leq t \leq T_c, \quad (1)$$

where

$$\phi(t) \triangleq 2\pi (f_L t_r(t) + m_c t_r^2(t)) \quad (2)$$

is the time varying phase of the carrier waveform, with $t_r(t) = t - \left\lfloor \frac{t}{T_{sw}} \right\rfloor T_{sw}$ being the periodic ramp function having period T_{sw} , $2m_c = \frac{f_H - f_L}{T_{sw}}$ is the chirp rate, $T_c = N_c T_{sw}$ is the total carrier duration, and N_c is the number of chirp pulses comprising the carrier waveform.

The message signal containing pilot and data symbols is:

$$s(t) = \sum_{k=0}^{N-1} s_k g(t - kT), \quad (3)$$

where $s_k, k = 0, \dots, N-1$, are a sequence of symbols drawn from a constant-modulus constellation such as quadrature phase shift keying (QPSK), T is the symbol duration, $N = \frac{T_c}{T}$ is the number of symbols in the data packet and $g(t)$ is a pulse shaping function, for example, a root-raised-cosine pulse with roll-off factor α . We denote the symbol bandwidth by B , which is given by $B \approx \frac{1+\alpha}{T}$. For a symbol interval $T (< T_{sw})$, we can mount up to $M = \lfloor T_{sw}/T \rfloor$ symbols within a chirp pulse. Note that there are $N = MN_c$ symbols in a data packet. For simplicity, we assume that T_{sw}/T is an integer.

The modulated transmit signal is given by

$$x(t) = \text{Re} [s(t)c(t)], \quad (4)$$

which is prefixed with a preamble pulse and appended with a post-amble pulse to form a transmission frame. The preamble and post-amble are used for timing and synchronization, and for estimating the channel. A guard interval of T_g is used after (before) the preamble (post-amble) pulse to facilitate channel estimation. Using $N_c > 1$ helps in amortizing the overhead due to the guard interval over the total carrier duration of T_c .

The time-varying impulse response of the UWA channel is modeled as [29]:

$$h(t, \tau) = \sum_{p=0}^{N_p-1} h_p(t) \delta(\tau - \tau_p(t)), \quad (5)$$

where $h_p(t)$ and $\tau_p(t)$ are the time-varying amplitude and delay, respectively, of the p th path, and N_p is the number of significant paths in the channel. The delay-scale model in (5) capture the effects of multipath propagation (i.e., reflection, scattering, and refraction) and the time variation of the propagation delays due to source-receiver motion, scattering by fluctuating ocean surfaces, and internal gravity waves such as interfacial waves and solitons within the fluid medium. As in [21]–[24], we assume that the path amplitudes are constant within a data packet, that is, $h_p(t) = h_p$, and that the time variation of the path delays due to Doppler rate a_p can be approximated as

$$\tau_p(t) = \tau_p - a_p t. \quad (6)$$

After coarse Doppler scale compensation and synchronization, the received signal is given by

$$y(t) = \sum_{p=0}^{N_p-1} y_p(t) + w(t), \quad (7)$$

where $w(t)$ is the additive white Gaussian noise (AWGN), $y_p(t) = h_p \text{Re}\{s(\tilde{t} - \tau_p(\tilde{t}))c(\tilde{t} - \tau_p(\tilde{t}))\}$ is the Doppler compensated and timing adjusted version of the S2C signal reaching via the p th path, $\tilde{t} = \frac{t + \hat{\tau}}{1 + \hat{a}}$ is the rescaled and shifted time-axis, \hat{a} is the coarse Doppler scale estimated using the preamble and post-amble as in [29], and $\hat{\tau}$ is the starting time instance of the first (data) chirp pulse estimated from the preamble/post-amble as in [6] but after resampling. Using (6), we can write,

$$y_p(t) = h_p \sum_{k=0}^{N-1} (s_{k,\text{Re}} \cos \phi_p(t) - s_{k,\text{Im}} \sin \phi_p(t)) g_{p,k}(t), \quad (8)$$

where $g_{p,k}(t) \triangleq g(\overline{1 + b_p t} - \tilde{\tau}_p - kT)$, with $b_p = \frac{a_p - \hat{a}}{1 + \hat{a}}$ and $\tilde{\tau}_p = \tau_p - (1 + b_p)\hat{\tau}$ being the residual Doppler scale and delay of the p th path after compensation, respectively, $s_{k,\text{Re}}$ ($s_{k,\text{Im}}$) is the real (imaginary) part of the symbol s_k , and $\phi_p(t) = \phi(\overline{1 + b_p t} - \tilde{\tau}_p)$ is the time-scaled and delayed version of the carrier phase in (2).

Upon sampling at a rate F_s ($= 1/T_s$, where T_s is the sampling period), we may re-express the received signal in (7) in a vector form relevant to data detection, as:

$$\mathbf{y} = \mathbf{H}\mathbf{s} + \mathbf{w}, \quad (9)$$

where

$$\begin{aligned} \mathbf{H} &= [C_0 \mathbf{h}, -S_0 \mathbf{h}, \dots, C_{N-1} \mathbf{h}, -S_{N-1} \mathbf{h}] \in \mathbb{R}^{NL \times 2N}, \\ \mathbf{h} &= [h_0, h_1, \dots, h_{N_p-1}]^T \in \mathbb{R}^{N_p \times 1}, \\ \mathbf{s} &= [s_{0,\text{Re}}, s_{0,\text{Im}}, \dots, s_{N-1,\text{Re}}, s_{N-1,\text{Im}}]^T \in \mathbb{R}^{2N \times 1}, \\ \mathbf{w} &\sim \mathcal{N}(\mathbf{0}, \sigma^2 I_{2N}), \end{aligned}$$

$L = \lfloor F_s T \rfloor$ is the number of samples in the symbol duration, $C_k \in \mathbb{R}^{NL \times N_p}$ and $S_k \in \mathbb{R}^{NL \times N_p}$ are matrices whose entries

are given by $C_k(l, p) = \cos \phi_p(lT_s) g_{p,k}(lT_s)$ and $S_k(l, p) = \sin \phi_p(lT_s) g_{p,k}(lT_s)$, for $0 \leq k \leq N-1$, $0 \leq l \leq NL-1$ and $0 \leq p \leq N_p-1$, and I_{2N} denotes the $2N \times 2N$ identity matrix. Since $g(t) = 0, t \notin [0, T]$, entries of $C_k(:, p) \in \mathbb{R}^{NL \times 1}$ and $S_k(:, p) \in \mathbb{R}^{NL \times 1}$ are zeros except for $l \in \left\{ \left\lfloor \frac{\tilde{\tau}_p + kT}{1 + b_p T_s} \right\rfloor, \dots, \left\lfloor \frac{\tilde{\tau}_p + k + 1T}{1 + b_p T_s} \right\rfloor \right\}$.

We now address the problem of data detection for the S2C communication model. First, we examine the two existing S2C receivers in the literature – the gradient heterodyne (GradH) receiver, pioneered in [6], and the path-based gradient heterodyne (pGradH) receiver proposed in [17].

III. EXISTING S2C RECEIVERS: GRADH AND PGRADH

We show that the GradH and pGradH based S2C receivers are minimum mean square error (MMSE) symbol detectors for the AWGN channel and a delay spread channel with well resolved path delays, respectively. We then introduce the reduced data measurement model, at the output of the GradH and pGradH preprocessors, that will be used in this work.

A. Optimality of GradH Receiver

Consider the received signal for the AWGN channel ($N_p = 1, \tilde{\tau}_0 = 0, b_0 = 0, h_0 = 1$), given by

$$y(t) = \sum_{k=0}^{N-1} (s_{k,\text{Re}} \cos \phi(t) - s_{k,\text{Im}} \sin \phi(t)) g(t - kT) + w(t).$$

Upon sampling, the received signal is as in (7) with the channel matrix taking the block-diagonal form $\mathbf{H} = \mathbf{Q} = \text{diag}\{Q_0, Q_1, \dots, Q_{N-1}\} \in \mathbb{R}^{NL \times 2N}$, where,

$$Q_k = \text{diag}(\mathbf{g}) \begin{bmatrix} \cos \phi^{(k)}[0] & \sin \phi^{(k)}[0] \\ \cos \phi^{(k)}[1] & \sin \phi^{(k)}[1] \\ \vdots & \vdots \\ \cos \phi^{(k)}[L-1] & \sin \phi^{(k)}[L-1] \end{bmatrix} \in \mathbb{R}^{L \times 2},$$

$\mathbf{g} = [g(0), g(T_s), \dots, g(\overline{(L-1)T_s})]^T \in \mathbb{R}^L$, and $\phi^{(k)}[l] = \phi(\overline{(\tilde{k} - 1)T + lT_s})$, $\tilde{k} = k - \lfloor \frac{k}{M} \rfloor M$, $l = 0, \dots, L-1$, $k = 0, 1, \dots, N-1$. In this case, there is no inter-symbol interference (ISI), and the measurement corresponding to the k th symbol is given by

$$\mathbf{y}_k = Q_k \mathbf{s}_k + \mathbf{w}_k, \quad (10)$$

where, for $k = 0, \dots, N-1$,

$$\begin{aligned} \mathbf{y}_k &= [y[(k-1)L], y[(k-1)L+1], \dots, y[kL-1]]^T, \\ \mathbf{s}_k &= [s_{k,\text{Re}}, s_{k,\text{Im}}]^T \in \left\{ \left[\pm 1/\sqrt{2}, \pm 1/\sqrt{2} \right]^T \right\}, \\ \mathbf{w}_k &= [w_k[0], \dots, w_k[L-1]]^T \sim \mathcal{N}(\mathbf{0}, \sigma^2 I_L). \end{aligned}$$

For equiprobable symbols s_k , the MAP solution to (10) is the same as the ML estimator, and is given by

$$\hat{\mathbf{s}}_k^{(\text{ML})} = \arg \min_{\mathbf{s}_k \in \left\{ \left[\pm 1/\sqrt{2}, \pm 1/\sqrt{2} \right]^T \right\}} \|\mathbf{y}_k - Q_k \mathbf{s}_k\|_2, \quad (11)$$

and the MMSE solution to (10) is given by

$$\hat{\mathbf{s}}_k^{(\text{MMSE})} = \mathcal{S} \left[(Q_k^T Q_k + \sigma^2 I_2)^{-1} Q_k^T \mathbf{y}_k \right], \quad (12)$$

where $\mathcal{S}[\cdot]$ is the slicing operation that quantizes each entry of its argument vector to the nearest symbol in the QPSK constellation.

Suppose the symbol time T (and hence L) is sufficiently large and the pulse shaping function, $g(t)$, is smooth, so that the following holds for all $0 \leq k \leq N - 1$:

$$\sum_{l=0}^{L-1} g^2(lT_s) \cos^2(\phi^{(k)}[l]) \approx \sum_{l=0}^{L-1} g^2(lT_s) \sin^2(\phi^{(k)}[l]) \approx \beta,$$

and

$$\frac{1}{\beta} \sum_{l=0}^{L-1} g^2(lT_s) \cos(\phi^{(k)}[l]) \sin(\phi^{(k)}[l]) \approx 0,$$

where $\beta \triangleq \frac{1}{2} \sum_{l=0}^{L-1} g^2(lT_s)$. Then, we have $Q_k^T Q_k \approx \beta I_2$. To observe the goodness of this approximation, consider the S2C system in Table I, $L = 50$ raw samples per symbol, and a root-raised cosine pulse shaping function $g(t)$ with a roll-off $\alpha = 0.25$ and truncated to the symbol span. The diagonal entries of $Q_k^T Q_k$ differ by at most 0.09 dB, since

$$\max_k \frac{1}{\beta} \left| \sum_{l=0}^{L-1} g^2(lT_s) \cos(2\phi^{(k)}[l]) \right| < 0.02,$$

and the off-diagonal entries are at least -20 dB down compared to diagonal entries, since

$$\max_k \frac{1}{\beta} \left| \sum_{l=0}^{L-1} g^2(lT_s) \cos(\phi^{(k)}[l]) \sin(\phi^{(k)}[l]) \right| < 0.01.$$

Under these conditions, the MMSE receiver in (12) simplifies to the symbol-by-symbol decoder:

$$\hat{\mathbf{s}}_k^{(\text{GradH})} = \mathcal{S}[\mathbf{z}_k], \quad (13)$$

where $\mathbf{z}_k = Q_k^T \mathbf{y}_k$. Note that Q_k can be viewed as a lowpass filter, and there is a decimation by a factor of L in going from \mathbf{y}_k to \mathbf{z}_k . From (10), we see that $\mathbf{z}_k \approx \beta \mathbf{s}_k + \mathbf{v}_k$, where $\mathbf{v}_k = Q_k^T \mathbf{w}_k \sim \mathcal{N}(\mathbf{0}, \beta \sigma^2 I_2)$, is affected only by the k th symbol. Also, \mathbf{z}_k is a sub-vector of $\mathbf{z} = Q^T \mathbf{y} \in \mathbb{R}^{2N \times 1}$, whose entries are precisely the sampled versions of the lowpass filtered in-phase and quadrature outputs of gradient heterodyne operation, as in [6], on the received signal. Therefore, the GradH receiver in [6] realizes a near MMSE decoder for S2C communication over an AWGN channel.

While the GradH receiver in (13) is an MMSE symbol detector for the AWGN channel, the receiver works reasonably well even for ISI channels with *moderate* delay spreads, as elaborated in [6]. It is shown in [17] that the GradH receiver recovers the symbol arriving along the *direct path* when

$$\frac{\mathcal{M}}{\mathcal{M}-1} \delta\tau_{\max} \leq T_{sw} \leq \mathcal{M} \delta\tau_{\min}, \quad (14)$$

where $\delta\tau_{\min} = \min_{0 \leq i < j \leq N_p - 1} |\tau_i - \tau_j|$ and $\delta\tau_{\max} = \max_{0 \leq i, j \leq N_p - 1} |\tau_i - \tau_j|$ are the smallest and largest separation between any two path arrival times τ_i and τ_j , and $\mathcal{M} \triangleq \frac{f_H - f_L}{B}$ is called the spreading factor.

B. Optimality of pGradH Receiver

The pGradH receiver in [17] combines the symbol arriving along paths other than the direct path to leverage multipath diversity in addition to the gradient heterodyne and lowpass filtering operation. Here, we show that pGradH is a near MMSE decoder when the path delays are well resolved and condition (14) holds.

For a given channel H , the MMSE receiver is given by

$$\hat{\mathbf{s}}^{(\text{MMSE})} = \mathcal{S} \left[\left(H^T H + \sigma^2 I_{2N} \right)^{-1} H^T \mathbf{y} \right]. \quad (15)$$

When condition (14) holds, $C_i^T C_j \approx \kappa_C I_{N_p} \delta_{i,j}$, where $\kappa_C = C_i(:, p)^T C_i(:, p)$ is nearly the same for all $0 \leq i \leq N - 1$ and $0 \leq p \leq N_p - 1$, and $\delta_{i,j}$ is the Kronecker delta function. Similarly, $S_i^T S_j \approx \kappa_S I_{N_p} \delta_{i,j}$, where $\kappa_S = S_i(:, p)^T S_i(:, p)$, and $C_i^T S_j \approx 0$. Under these approximations, the MMSE receiver in (15) simplifies to the pGradH receiver in [17],

$$\hat{\mathbf{s}}_k^{(\text{pGradH})} = \mathcal{S} \left[\sum_{p=0}^{N_p-1} \frac{h_p}{|h_p|^2} \mathbf{z}_k^{(p)} \right], \quad (16)$$

where

$$\mathbf{z}_k^{(p)} = Q_k^{(p)T} \mathbf{y}_k, \quad (17)$$

$$Q_k^{(p)} = \text{diag}(\mathbf{g}^{(p)}) \begin{bmatrix} \cos \phi_p^{(k)}[0] & \sin \phi_p^{(k)}[0] \\ \cos \phi_p^{(k)}[1] & \sin \phi_p^{(k)}[1] \\ \vdots & \vdots \\ \cos \phi_p^{(k)}[L-1] & \sin \phi_p^{(k)}[L-1] \end{bmatrix},$$

$\mathbf{g}^{(p)} \in \mathbb{R}^L$ has entries that are samples of the compressed/dilated and delayed pulse shaping function, $g_l^{(p)} = g(\overline{1 + b_p} l T_s - \tilde{\tau}_p)$, $\phi_p^{(k)}[l] = \phi_p((\tilde{k} - 1)T + lT_s)$, $\tilde{k} = k - \lfloor \frac{k}{M} \rfloor M$, $l = 0, \dots, L - 1$, $p = 0, \dots, N_p - 1$, and $k = 0, 1, \dots, N - 1$. Stacking up $\mathbf{z}_k^{(p)}$, $k = 0, 1, \dots, N - 1$, into a vector, we get

$$\mathbf{z}^{(p)} = Q^{(p)T} \mathbf{y} \in \mathbb{R}^{2N \times 1}, \quad (18)$$

where $Q^{(p)} = \text{diag}\{Q_0^{(p)}, Q_1^{(p)}, \dots, Q_{N-1}^{(p)}\} \in \mathbb{R}^{NL \times 2N}$. The entries of $\mathbf{z}^{(p)}$ are sampled versions of the lowpass filtered in-phase and quadrature outputs of *path-matched* gradient heterodyne operation, as in [17], on the received signal.

C. Reduced Data Measurement Model

We now present the data model for measurements, at *symbol rate*, at the output of the GradH and pGradH preprocessors. Henceforth, we use this reduced data measurement model instead of the raw signal samples at receiver front-end sampling rate, F_s , in (9).

The measurements at the output of GradH preprocessing, i.e., gradient heterodyne operation and lowpass filtering, can be written in the form

$$\mathbf{z} = G\mathbf{s} + \mathbf{v}, \quad (19)$$

where $G = Q^T H \in \mathbb{R}^{2N \times 2N}$ is the channel matrix at the output of the GradH preprocessor and lowpass filter, and $\mathbf{v} = Q^T \mathbf{w} \sim \mathcal{N}(\mathbf{0}, \sigma^2 Q^T Q)$. In the special case of an AWGN channel (i.e., $H = Q$), with a large enough symbol

duration T and smoothly varying pulse shaping function $g(t)$, the channel matrix $G = Q^T Q \approx \beta I_{2N}$ is nearly diagonal and $\mathbf{v} \sim \mathcal{N}(\mathbf{0}, \beta\sigma^2 I_{2N})$, as shown in Sec. III-A.

The measurement model at the output of pGradH preprocessing assumes the same form as in (19), where $\mathbf{z} \in \mathbb{R}^{2N}$ is the output of the MRC processor given by $\mathbf{z} = \sum_{p=0}^{N_p-1} \frac{h_p}{|h_p|^2} \mathbf{z}^{(p)}$, $G = \sum_{p=0}^{N_p-1} \frac{h_p}{|h_p|^2} G^{(p)} \in \mathbb{R}^{2N \times 2N}$ is the effective channel matrix at the output of the MRC processor, $G^{(p)} = Q^{(p)T} H \in \mathbb{R}^{2N \times 2N}$ is the channel matrix at the output of the p th branch of the pGradH preprocessor, $\mathbf{v} = \sum_{p=0}^{N_p-1} \frac{h_p}{|h_p|^2} \mathbf{v}^{(p)} \in \mathbb{R}^{2N}$ and $\mathbf{v}^{(p)} = Q^{(p)T} \mathbf{w} \sim \mathcal{N}(\mathbf{0}, \sigma^2 Q^{(p)T} Q^{(p)})$. For a moderately delay spread channel with well resolved path delays and large symbol duration, $Q^{(p)T} Q^{(q)} \approx \beta \delta_{p,q} I_{2N}$, $0 \leq p, q \leq N_p - 1$ due to (14). In this case, $G^{(p)} \approx \beta h_p I_{2N}$, $\mathbf{v}^{(p)} \sim \mathcal{N}(\mathbf{0}, \beta\sigma^2 I_{2N})$, and therefore G , the channel matrix at the output of the GradH and pGradH preprocessors, is nearly diagonal.

In the next section, we bring out the need to consider alternate S2C receiver processing in large delay spread channels.

IV. LIMITATIONS OF GRADH AND PGRADH RECEIVERS

For both GradH and pGradH receivers, the condition in (14) is needed to ensure that the ISI is negligible after gradient heterodyne operation and lowpass filtering. The condition (14) places a *lower limit* on the minimum differential path delay, $\delta\tau_{\min}$, of the multipath arrivals to avoid ISI ensuing from the mixing of adjacent symbols at the GradH and pGradH preprocessor outputs [17]. The condition (14) also places an *upper limit* on the channel delay spread, $\delta\tau_{\max}$, to avoid interference between the symbols on the corresponding frequency sweep slots of different chirp pulses. Together, these limits require the symbol rate, $R = 1/T$, of the existing S2C receivers to satisfy

$$R \leq \left(\frac{f_H - f_L}{1 + \alpha} \right) \frac{\min\{\delta\tau_{\min}, T_{\text{sw}} - \delta\tau_{\max}\}}{T_{\text{sw}}}. \quad (20)$$

The upper limit on the achievable rate, in (20), is maximized when $T_{\text{sw}} = \delta\tau_{\max} + \delta\tau_{\min}$, and the maximum rate achievable by the existing S2C receivers is given by

$$R_{\max} = \left(\frac{f_H - f_L}{1 + \alpha} \right) \frac{\delta\tau_{\min}}{\delta\tau_{\max} + \delta\tau_{\min}}. \quad (21)$$

Note that the rate limiting condition $R \leq R_{\max}$ to avoid ISI at the preprocessor output of the existing S2C receivers, is equivalent to imposing a lower bound on the spreading factor: $\mathcal{M} \geq \frac{\delta\tau_{\max}}{\delta\tau_{\min}} + 1$. When the system is operated at a symbol rate $R = R_{\max}$, the spreading factor $\mathcal{M} = \frac{\delta\tau_{\max}}{\delta\tau_{\min}} + 1$.

Existing S2C receivers entail ISI when operating at a symbol rate greater than R_{\max} . Consider, for example, the S2C system in Table I operating in a UWA channel simulated in Sec. VI-B1. There are 20 QPSK symbols (i.e., 40 bits) in one chirp pulse (S2C block) of duration $T_{\text{sw}} = 10$ ms. Figure 1 shows a transmitted S2C frame, where the symbols $s_{i,j}$ and $s_{i,j+1}$ can potentially interfere with the detection of $s_{i,j+2}$, $j = 1, 2, 3$. Figures 2 and 3 display the images of the raw channel matrix H , in (9), and the corresponding effective channel G , in (19), respectively. Yellow pixels show

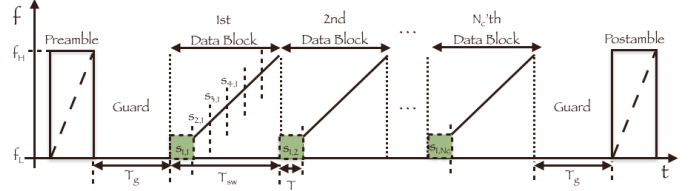


Fig. 1. An S2C frame consisting of preamble, N_c chirp pulses (data blocks), and post-amble. Although $T \geq \frac{1}{\sqrt{2m_c}}$ avoids ISI among adjacent symbols, inter-block interference (IBI) among the symbols mounted on the same frequency sweep slots (green slots) can happen if T_{sw} is smaller than the channel delay spread.

the large magnitude entries in the visual images of $|H|$ and $|G|$. Large magnitude off-diagonal entries lead to ISI. Compared to the raw channel matrix H , the effective channel G after gradient heterodyne and lowpass filtering exhibit reduced ISI. This is shown by the relatively weaker (blue) off-diagonal entries of $|G|$. The gradient heterodyne and lowpass filtering operation has reduced the strength of the off-diagonal entries in G that contribute to ISI among symbols within a chirp pulse (intra-block interference). But, strong residual inter-block interference remains at the GradH/pGradH preprocessor output as shown by the large magnitude (yellow) pixels around $G_{i,i-40}$, $40 < i \leq 2N$, in Figure 3. In turn, this adversely affects the performance of the existing S2C receivers in a severely delay spread UWA channel. In such channels, existing S2C receivers must compromise on the data rate in order to restore the symbol recovery performance.

In the following section, we consider alternate receivers for S2C communications that can handle channel delay spreads greater than the chirp pulse duration and work well for symbol rates higher than the upper limit on the data rate, R_{\max} .

V. VARIATIONAL SOFT SYMBOL DECODER (VSSD)

We now develop a symbol detector based on the variational Bayes' inference that approximates the optimum MAP decoder and offers significantly improved performance over the MMSE receiver. The development of the VSSD is the main contribution of this work.

The optimum (MAP) decoder outputs the symbol vector $\mathbf{s} \in \mathcal{P} = \{-\frac{1}{\sqrt{2}}, +\frac{1}{\sqrt{2}}\}^{2N}$ that maximizes the posterior $p(\mathbf{s}|G, \mathbf{z}) = p(\mathbf{z}|G, \mathbf{s})p(\mathbf{s})/p(\mathbf{z}|G)$. Direct maximization of the posterior requires a computationally intensive search over 2^{2N} lattice points in \mathcal{P} . Computing the posterior symbol probabilities, which in turn yield the soft symbols to be input to the channel decoder, is also hard since the marginalization over \mathbf{s} in $p(\mathbf{z}|G) = \sum_{\mathbf{s} \in \mathcal{P}} p(\mathbf{s}, \mathbf{z}|G)$ is involved. We instead seek a good approximation to the posterior, $q_\phi(\mathbf{s}|G, \mathbf{z})$, called the variational decoder. Here, ϕ represents the model parameters whose values are estimated based on the variational inference principle, as explained below.

To make the problem tractable, we assume that the approximate posterior is fully factorizable:

$$q_\phi(\mathbf{s}|G, \mathbf{z}) = \prod_{k=0}^{N-1} q_\phi(s_{k,\text{Re}}|G, \mathbf{z}) q_\phi(s_{k,\text{Im}}|G, \mathbf{z}). \quad (22)$$

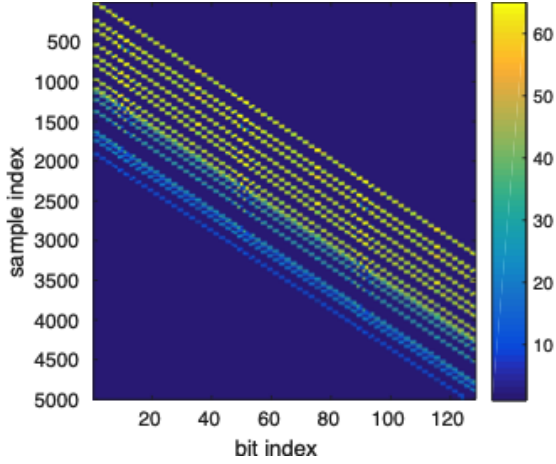


Fig. 2. Channel matrix image, $|H| \in \mathbb{R}^{NL \times 2N}$, before GradH processing. Pixel intensities are in linear units and only the portion corresponding to first 128 bits is shown. For the purpose of visualization, $|H|$ is scaled such that the median of the entire of its scaled version assumes a value of $\frac{1}{6}$ on the color bar shown.

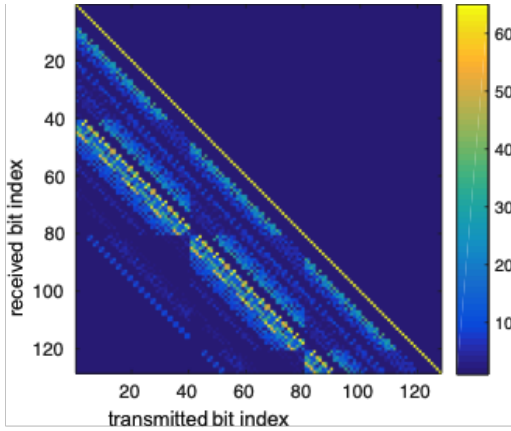


Fig. 3. Channel matrix image, $|G| \in \mathbb{R}^{2N \times 2N}$, after GradH processing. Pixel intensities are in linear units and only the portion corresponding to first 128 bits is shown. For the purpose of visualization, $|G|$ is scaled such that the median of the entire of its scaled version assumes a value of $\frac{1}{6}$ on the color bar shown.

Following Kingma et al. [30], the evidence lower bound (ELBO) on the log likelihood of the observation is given by

$$\mathcal{L}(\theta, \phi, \mathbf{z}) = \mathbb{E}_{q_{\phi}(\mathbf{s}|G, \mathbf{z})} \log p_{\theta}(\mathbf{z}|G, \mathbf{s}) - \mathbb{E}_{q_{\phi}(\mathbf{s}|G, \mathbf{z})} \left[\log \frac{q_{\phi}(\mathbf{s}|G, \mathbf{z})}{p_{\theta}(\mathbf{s})} \right], \quad (23)$$

where $\log p_{\theta}(\mathbf{z}|G, \mathbf{s})$ is the likelihood function and $p_{\theta}(\mathbf{s})$ is a prior on the symbol vector.

To bring $q_{\phi}(\mathbf{s}|G, \mathbf{z})$ close to $p(\mathbf{s}|G, \mathbf{z})$, we maximize the ELBO, $\mathcal{L}(\theta, \phi, \mathbf{z})$. The ELBO consists of the likelihood term

$$\mathbb{E}_{q_{\phi}(\mathbf{s}|G, \mathbf{z})} \log p_{\theta}(\mathbf{z}|G, \mathbf{s}) = -N \log(2\pi\sigma^2) - \mathbb{E}_{q_{\phi}(\mathbf{s}|G, \mathbf{z})} \left[\frac{\|\mathbf{z} - G\mathbf{s}\|^2}{2\sigma^2} \right], \quad (24)$$

and the regularizing term,

$$\mathbb{E}_{q_{\phi}(\mathbf{s}|G, \mathbf{z})} \left[\log \frac{q_{\phi}(\mathbf{s}|G, \mathbf{z})}{p_{\theta}(\mathbf{s})} \right] = KL(q_{\phi}||p_{\theta}). \quad (25)$$

We assume a simple uniform prior $p_{\theta}(\mathbf{s}) = \frac{1}{2^{2N}}$. Therefore, when maximizing ELBO, the regularizing term acts to penalize the departure of the variational approximation q_{ϕ} from the uniform prior. On maximizing the ELBO, we get the following fixed point equations (see appendix for details):

$$\mathbf{q} = \varphi(\boldsymbol{\alpha}), \quad (26)$$

where

$$\begin{aligned} \alpha_j &= \frac{\sqrt{2}}{\sigma^2} \left(\mathbf{z}^T G_{:,j} - \sum_{l=0}^{2N-1} G_{l,j} \left(\sum_i v_{l,i} - v_{l,j} \right) \right), \\ v_{l,j} &= \frac{1}{\sqrt{2}} G_{l,j} (2q_j - 1), \\ \varphi(\alpha_j) &= \frac{1}{1 + e^{-\alpha_j}}, \end{aligned} \quad (27)$$

for $j = 1, \dots, 2N - 1$.

Note that the fixed point iterations lead to *soft symbol* estimates in the form of the probability vector \mathbf{q} . We perform symbol detection by slicing the probability vector in uncoded communications. In coded communications, the soft symbols are converted to LLRs and fed to the channel decoder.

The fixed point updates do not involve any matrix inversions and their computational complexity, $\mathcal{O}(N^2)$, is an order of magnitude smaller than the computational complexity, $\mathcal{O}(N^3)$, of the MMSE receiver.

Special Channels: It is insightful to specialize the fixed point iterations for some simple channel models. Consider the case when the channel matrix is orthogonal, i.e.,

$$G_{:,i}^T G_{:,j} = \|G_{:,i}\|_2^2 \delta_{i,j}.$$

Note that the AWGN channel and Rayleigh fading channel are examples of orthogonal channels. In this case, the fixed point iterations in (26) reduce to the following one point update:

$$\mathbf{q} = \frac{1}{1 + e^{-\left(\frac{\sqrt{2}}{\sigma^2} G^T \mathbf{z}\right)}}. \quad (28)$$

Therefore, deciding the hard symbols from the probability vector \mathbf{q} is tantamount to slicing the matched filtered observation: $\tilde{\mathbf{z}} = G^T \mathbf{z}$. Deciding $s_k = \pm \frac{1}{\sqrt{2}}$ based on $q_k \geq 0.5$ is equivalent to that based on $\tilde{z}_k \geq 0$. In other words, VSSD is an ML decoder for orthogonal channels.

Convergence: We show that every update of the fixed point iteration in (26) is along the gradient of the ELBO (ascent direction), and therefore cannot decrease the ELBO. To see this, consider the inner product of $\varphi(\boldsymbol{\alpha}) - \mathbf{q}$ and $\nabla \mathcal{L}$:

$$(\varphi(\boldsymbol{\alpha}) - \mathbf{q})^T \nabla \mathcal{L} = \sum_{j=0}^{2N-1} (\varphi(\alpha_j) - q_j) \nabla \mathcal{L}_j. \quad (29)$$

We show in the appendix (see equation (66)) that $\nabla \mathcal{L}_j = \alpha_j - \log q_j + \log(1 - q_j)$. Each term in (29) is nonnegative since $\varphi(\alpha_j) - q_j \geq 0 \Leftrightarrow \alpha_j - \log q_j + \log(1 - q_j) \geq 0$. Thus, the inner product is nonnegative and hence the update $\mathbf{q} \rightarrow \varphi(\boldsymbol{\alpha}(\mathbf{q}))$ cannot decrease ELBO. Further, for any channel matrix, the ELBO is upper bounded by the marginal log likelihood, $\log p_{\theta}(\mathbf{z})$. Therefore, the fixed point iterations always converge to a stationary point of the ELBO.

Next, we characterize the stationary points of the ELBO and elicit sufficient conditions that make these points a *global maximum*, *local maximum* or a *saddle point*.

Global Maximum: The entries of the Hessian matrix of \mathcal{L} with respect to \mathbf{q} , i.e., $\nabla_{\mathbf{q}}^2 \mathcal{L} \in \mathbb{R}^{2N \times 2N}$, are given by

$$\frac{\partial^2 \mathcal{L}}{\partial q_j^2} = -\frac{1}{q_j(1-q_j)} < 0, \quad (30)$$

$$\frac{\partial^2 \mathcal{L}}{\partial q_i \partial q_j} = \frac{\partial^2 \mathcal{L}}{\partial q_j \partial q_i} = -\frac{2}{\sigma^2} \sum_l G_{l,i} G_{l,j}, i \neq j, \quad (31)$$

where $i, j \in \{0, 1, \dots, 2N-1\}$. For orthogonal channel matrices, the matrix G satisfies $\sum_l G_{l,i} G_{l,j} = 0$, which makes the Hessian negative definite and therefore the stationary point \mathbf{q}_* a global maximizer of the ELBO.

A larger class of channel matrices for which global convergence is guaranteed can be found by requiring $-\nabla_{\mathbf{q}}^2 \mathcal{L}$ to be diagonally dominant, i.e.,

$$\eta_j \triangleq \frac{2}{\sigma^2} \sum_{i \neq j} \left| \sum_l G_{l,i} G_{l,j} \right| < \frac{1}{q_j(1-q_j)}, \forall j, \quad (32)$$

which implies:

$$q_j^2 - q_j + 1/\eta_j > 0, \forall j. \quad (33)$$

Now, the condition in (33) holds for every $0 \leq q_j \leq 1$ if and only if $0 \leq \eta_j < 4$. Note that $-\nabla_{\mathbf{q}}^2 \mathcal{L}$ is symmetric and all its diagonal entries are positive. Since diagonal dominance of $-\nabla_{\mathbf{q}}^2 \mathcal{L}$ implies its positive definiteness (p.d.), $-\nabla_{\mathbf{q}}^2 \mathcal{L}$ is p.d. for the class of channel matrices $\mathcal{G} = \{G \in \mathbb{R}^{2N \times 2N} : \sum_{i \neq j} |\sum_l G_{l,i} G_{l,j}| < 2\sigma^2, \forall j\}$ and therefore global convergence is guaranteed whenever $G \in \mathcal{G}$.

Local Maximum: If $G \in \mathcal{G}$, the limit point \mathbf{q}_* is a global maximizer. Or else, if $G \notin \mathcal{G}$ and $q_{j,*} \notin (\kappa_j^{(1)}, \kappa_j^{(2)}) \subset [0, 1], \forall j$, where $\kappa_j^{(1,2)}$ are the roots of the equation $q_j^2 - q_j + 1/\eta_j = 0$ ($\eta_j > 4$) given by

$$\kappa_j^{(1,2)} = \frac{1 \pm \sqrt{1 - 4/\eta_j}}{2}, \forall j, \quad (34)$$

then the limit point \mathbf{q}_* is a local maximum.

Either Local Maximum or Saddle Point: If $G \notin \mathcal{G}$ and $q_{j,*} \in (\kappa_j^{(1)}, \kappa_j^{(2)})$, for some j , then the limit point \mathbf{q}_* is either a local maximum or a saddle point.

Consider, for example, a channel matrix with i.i.d. $\mathcal{N}(0, 1)$ entries. The length of the interval $(\kappa_j^{(1)}, \kappa_j^{(2)})$ is given by

$$l_{N,j} = \kappa_j^{(2)} - \kappa_j^{(1)} = \sqrt{1 - 4/\eta_j}. \quad (35)$$

From the definition of η_j in (32), triangle inequality, and the i.i.d. property of the entries of G , we have:

$$\mathbb{E}[\eta_j] \leq \frac{2}{\sigma^2} \sum_{i \neq j} \sum_l \mathbb{E}[|G_{l,i}|] \mathbb{E}[|G_{l,j}|] = \frac{8N(2N-1)}{\pi\sigma^2}, \quad (36)$$

and therefore,

$$\mathbb{E}[l_{N,j}^2] = 1 - 4\mathbb{E}[1/\eta_j] \leq 1 - 4/\mathbb{E}[\eta_j] = 1 - \frac{\pi\sigma^2}{2N(2N-1)}, \quad (37)$$

TABLE I
S2C PARAMETERS USED IN THE SIMULATION.

Carrier frequency (f_c)	15 kHz
Bandwidth (W)	10 kHz
Chirp rate ($2m_c$)	1 MHz/s
Symbol duration (T)	0.5 ms
Sweep duration (T_{sw})	10 ms
Guard interval (T_g)	25 ms

where we used the fact that $\mathbb{E}[1/\eta_j] \leq 1/\mathbb{E}[\eta_j]$ which follows from Jensen's inequality and the convexity of $f(\eta) = 1/\eta, \eta > 0$. Since $\mathbb{P}\{\eta_j > 4\} \rightarrow 1$, as $N \rightarrow \infty$, for i.i.d. Gaussian channel matrices, the fixed point is in $(\kappa_j^{(1)}, \kappa_j^{(2)})$ with high probability. Furthermore, since for every $\delta > 0$, $\mathbb{P}\{l_{N,j}^2 > 1 - \delta\} \rightarrow 1$ as $N \rightarrow \infty$, we have $l_{N,j} \xrightarrow{P} 1$.

Since, in this case, \mathbf{q}_* could be a saddle point, we perturb \mathbf{q}_* so as to move out of the saddle region in an attempt to further increase the ELBO. If the ELBO is found to increase for a few attempts of random perturbation, we continue the iterations from the point yielding the highest ELBO.

Acceleration: Finally, we propose to accelerate the fixed point updates to achieve faster convergence. Specifically, we choose γ_n at the n th iterate so that the update,

$$\mathbf{q}_n = \mathbf{q}_{n-1} + \gamma_n [\varphi(\boldsymbol{\alpha}_{n-1}) - \mathbf{q}_{n-1}], \quad (38)$$

results in maximal increase of ELBO. The optimum value of γ_n can be found through a 1-D search over a bounded interval in \mathbb{R} . Specifically, the optimum value of γ_n in (38), that best increases ELBO, lies within $[\gamma_{\min}, \gamma_{\max}] \in \mathbb{R}$, with

$$\gamma_{\min} = \max \left\{ \max_{\varphi(\alpha_j) > q_j} \frac{-q_j}{\varphi(\alpha_j) - q_j}, \max_{\varphi(\alpha_j) < q_j} \frac{1 - q_j}{\varphi(\alpha_j) - q_j} \right\},$$

$$\gamma_{\max} = \min \left\{ \min_{\varphi(\alpha_j) < q_j} \frac{-q_j}{\varphi(\alpha_j) - q_j}, \min_{\varphi(\alpha_j) > q_j} \frac{1 - q_j}{\varphi(\alpha_j) - q_j} \right\}.$$

VI. NUMERICAL SIMULATIONS

We demonstrate the performance of VSSD in three different settings: the benchmark i.i.d. Gaussian multiple-input multiple-output (MIMO) channel, UWA channels simulated according to two different models in the literature, and real-world measured UWA channels. We define the signal to noise ratio (SNR) at the receiver as

$$\text{SNR} = \frac{E\{\|G\mathbf{s}\|_2^2\}}{E\{\|\mathbf{v}\|_2^2\}}. \quad (39)$$

A. IID Gaussian MIMO Channel

We generate the channel matrix G , with entries $G_{i,j} \stackrel{i.i.d.}{\sim} \mathcal{N}(0, 1)$. First, we evaluate the BER of the VSSD receivers for $N = 10, 100$ symbols, for the uncoded QPSK signaling, and with perfect channel knowledge. We terminate the VSSD iterations at the n th iteration if $\|\mathbf{q}_n - \mathbf{q}_{n-1}\|_2 < 10^{-3}$. Figure 4 shows the BER plots for different SNR values. For $N = 10$ symbols, we show the BER of the ML decoder obtained by using the soft sphere decoder (SSD) in [31], [32] and whose implementation is available in [33]. The VSSD

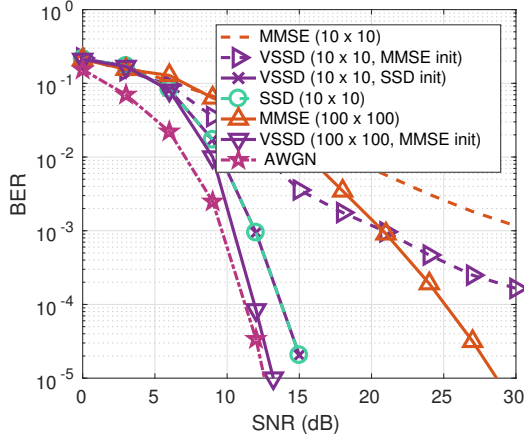


Fig. 4. BER of VSSD, SSD and MMSE receivers for i.i.d. Gaussian channel matrix ($N = 10, 100$) and AWGN channel.

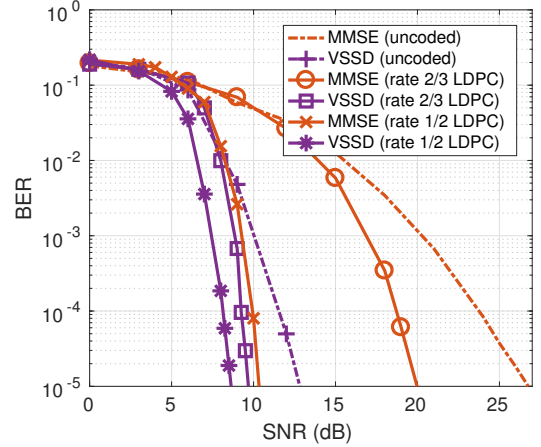


Fig. 5. BER of VSSD and MMSE receivers for i.i.d. Gaussian channel matrix.

receiver, initialized with the soft symbol estimate of SSD, retains the SSD's optimum (ML) performance, as expected. When initialized with the MMSE estimate of the symbol vector, VSSD outperforms the MMSE receiver by a margin of about 8-9 dB at a BER of 10^{-3} for $N = 10$. Note that, while SSD outperforms VSSD for $N = 10$, sphere decoding is not practical at large values of N due to its high computational complexity.¹ Moreover, for $N = 100$, the performance of the VSSD receiver on the i.i.d. Gaussian MIMO channel is close to that on an AWGN channel. On the AWGN channel, all receivers perform equally well, as expected.

In Figure 5, we compare the BER of the receivers for $N = 288$ symbols, for uncoded and coded QPSK communications, assuming perfect channel knowledge. For coded communication, we use a rate 1/2 and rate 2/3 LDPC code from [34]. In uncoded communication, the VSSD receiver achieves a BER of 10^{-3} at about 10 dB lower SNR than the MMSE receiver. In the rate 2/3 (1/2) coded communication, for a BER of 10^{-3} , VSSD outperforms MMSE receiver by an SNR margin of 8 dB (2 dB). For the same BER (10^{-3}), the VSSD receiver with a rate 2/3 code works at about 1 dB lower SNR than the MMSE receiver with a rate 1/2 code. Therefore, VSSD receiver offers 33% higher data rate than the MMSE receiver, while achieving the same BER.

Next, we consider the effect of imperfect channel knowledge due to channel estimation error on the BER. To do so, we perturb the entries of the i.i.d. Gaussian channel matrix with i.i.d. Gaussian noise, i.e. $G_{i,j} = G_{i,j} + \epsilon_{i,j}$, where $\epsilon_{i,j} \sim \mathcal{N}(0, \Delta)$, $1 \leq i, j, \leq 2N$. Figure 6 shows the BER of VSSD and MMSE decoders for $\Delta = 1/4, 1/5$ and coded communications using a rate 2/3 LDPC code. VSSD receiver retains its performance advantage over MMSE even with channel estimation errors.

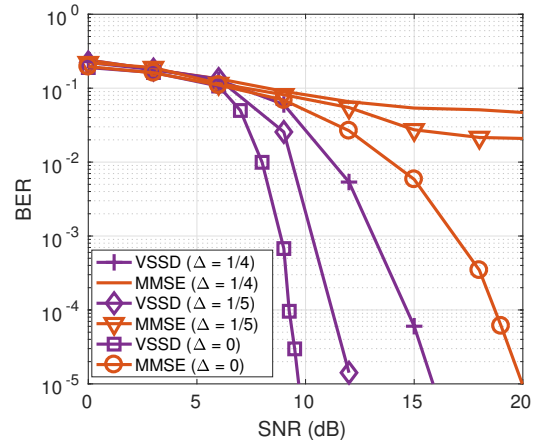


Fig. 6. BER of VSSD and MMSE receivers, under channel estimation errors, for i.i.d. Gaussian channel matrix.

B. Simulated UWA Channels

We now consider the performance of VSSD based receiver for the S2C communication system in Table I over a simulated UWA channel. Note that the symbol rate that is two times the upper limit, $R_* = \sqrt{2m_c} = 1$ kHz, on the existing S2C receivers.² A total of $N = 288$ QPSK symbols are mounted on a train of $N_c = 15$ chirp pulses. We investigate the performance for two models of UWA channels.

1) *Model I:* The first UWA channel model we consider is as in [21], [22] and used by numerous researchers in the field. The channel is generated with $N_p = 16$ discrete paths whose inter-arrival times are exponentially distributed with a mean of 1 ms. The Doppler rates are uniformly distributed in $[-b_{\max}, b_{\max}]$, where $b_{\max} = 5 \times 10^{-4}$. The path amplitudes are Rayleigh distributed with the average power decreasing exponentially with delay, where the difference between the beginning and the end of the guard time is 20 dB. Notice that neither of the narrowband approximation conditions [20] $B/f_c \ll 1$ or $b_{\max} \ll 1/BT$ are met in this case. Therefore,

¹On a 2.4 GHz Intel Xeon(R) processor, SSD takes 4.5 s on average to decode $N = 20$ symbols at SNR = 10 dB. For $N = 30$ symbols and at the same SNR, decoding does not finish within 5 minutes.

²Adjacent symbol interference, within a chirp pulse, is avoided in existing S2C receivers only if $2m_c T \geq B \approx \frac{1+\alpha}{T} \Rightarrow R \leq \sqrt{\frac{2m_c}{1+\alpha}} \leq \sqrt{2m_c} \triangleq R_*$.

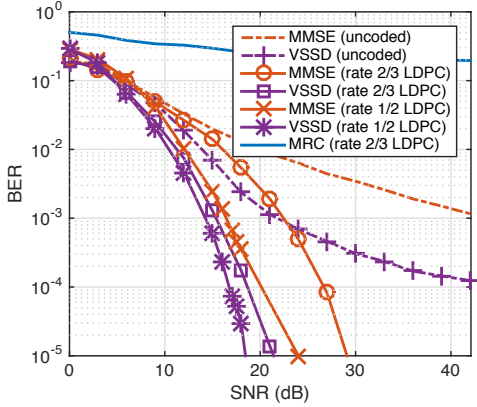


Fig. 7. BER of VSSD and MMSE receivers over a UWA channel simulated according to the model in Berger et al. [21].

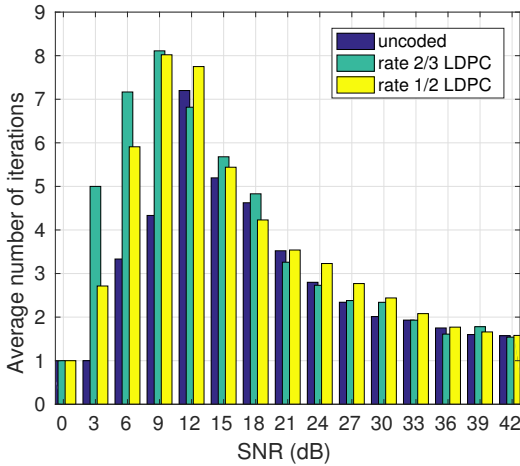


Fig. 8. Number of VSSD iterations averaged over 1000 trials for each SNR.

it is pertinent to evaluate the symbol recovery schemes based on the system model (9) for S2C communications over such a wideband delay-scale channel.

Figure 7 shows the BER of the MRC [17], VSSD and MMSE based data detection assuming perfect channel knowledge. The MRC receiver has completely failed due to severe ISI at pGradH preprocessor output (see Figure 3). Again, from these plots, we notice a strong performance of the VSSD based symbol detection in an S2C receiver. The VSSD receiver attains a $\text{BER} = 10^{-3}$ at about 18 dB lower SNR than MMSE in uncoded communication. In coded communication, the SNR margin of VSSD over the MMSE receiver is 8 dB (3 dB) for rate 2/3 (1/2) LDPC code.

Figure 8 shows the number of VSSD iterations (averaged over at least 1000 trials) for different SNR. On an average, the number of iterations stay below 10 and the maximum number of iterations never crossed 15.

2) *Model II*: We consider the UWA channel model proposed in [35]. The acoustic channel simulator code, available at [36], is used for generating the time-varying channel. Table II lists the parameters of the channel. A sample realization of the time-varying channel impulse response is shown in

TABLE II
UNDERWATER CHANNEL SIMULATION PARAMETERS.

Ocean depth (m)	100
Transmitter depth (m)	90
Receiver depth (m)	50
Channel distance (m)	1000
Spreading factor	1.7
Sound speed in water, c_w (m/s)	1500
Sound speed in bottom, c_b (m/s)	1200
Surface variance, σ_s^2 (m ²)	1.125
Bottom variance, σ_b^2 (m ²)	0.5
3 dB width of the PSD of intra-path delays, $B_{\delta,p}$ (Hz)	0.05
Number of intra-paths, S_p	20
Mean of intra-path amplitudes, μ_p	0.3
Variance of intra-path amplitudes, ν_p	10^{-4}
Transmitter drifting speed, v_{td} (m/s)	0.3
Transmitter drifting angle, θ_{td} (rad)	$\mathcal{U}(0, 2\pi)$
Receiver drifting speed, v_{rd} (m/s)	0.1
Receiver drifting angle, θ_{rd} (rad)	$\mathcal{U}(0, 2\pi)$
Transmitter vehicular speed, v_{tv} (m/s)	$\mathcal{N}(0, 1)$
Transmitter vehicular angle, θ_{tv} (rad)	$\mathcal{U}(0, 2\pi)$
Receiver vehicular speed, v_{rv} (m/s)	-3
Receiver vehicular angle, θ_{rv} (rad)	$\mathcal{U}(0, 2\pi)$
Surface variation amplitude, A_w (m)	0.9
Surface variation frequency, f_w (mHz)	0.6

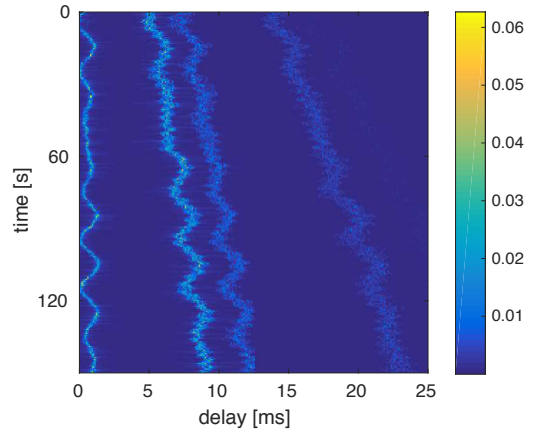


Fig. 9. Acoustic channel impulse response based on model in [35]. The first, second and third arrivals from the left correspond to the direct, bottom-reflected, and surface-reflected paths, respectively. The last arrival corresponds to a multiply reflected surface-bottom arrival.

Figure 9. Figure 10 shows an instance of the channel matrix (G) at the output of S2C preprocessing during the UWA channel simulation run. The inter symbol interference for this UWA channel is milder than the channel simulated according to the model in [21] (see Figure 3). Figure 11 shows the BER plots of the VSSD and MMSE receivers with and without channel errors. VSSD maintains a significantly better performance than MMSE decoder, as before.

C. WATERMARK Channels

The underWater Acoustic channel Replay benchMARK (WATERMARK) is a publicly available realistic simulation tool that comes packaged with five measured UWA channels [37], [38]. We use two of channel datasets, NOF1 and NCS1, that present two contrasting environments in the Norwegian seas [39]. The NOF1 channel is a Fjord in a shallow stretch of

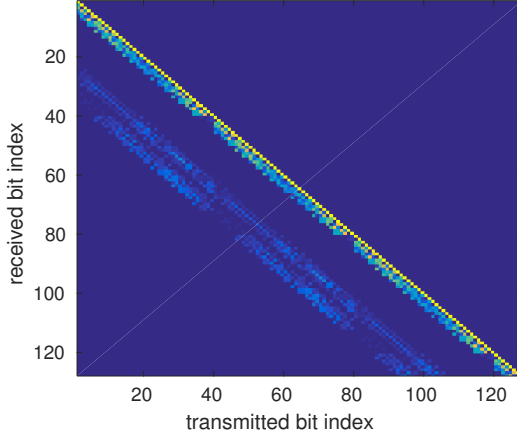


Fig. 10. Channel matrix after GradH processing at an instance during the simulation run of the UWA channel model in [35].

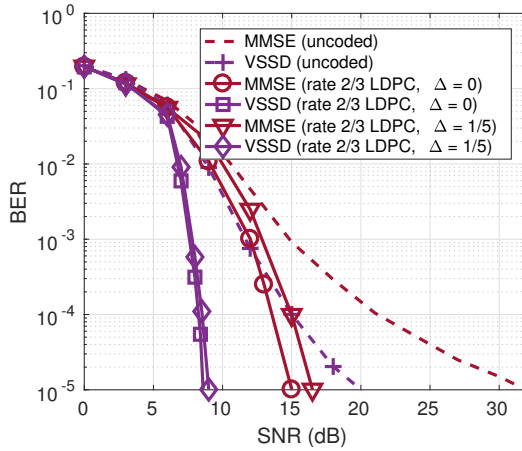


Fig. 11. BER of VSSD and MMSE receivers for S2C communications over UWA channel simulated according to [35].

Oslofjorden, and the NCS1 channel is a continental shelf in the Norwegian sea. The measured time-varying channel impulse responses include the effects of system hardware impairments such as clock frequency offset, sampling jitter etc, apart from the acoustic propagation effects.

Channel Matrix Computation: We first relate the complex baseband form of the measured channel impulse response data in WATERMARK, denoted by $h_B(t, \tau)$, and the channel matrix, G , at the output of the gradient heterodyne and lowpass filtering operation. Towards that end, we start with the baseband transmitted signal, given by

$$x_B(t) = s(t)c(t)e^{-j2\pi f_c t}. \quad (40)$$

The received baseband signal is given by

$$y_B(t) = \int_{\tau_{\min}(t)}^{\tau_{\max}(t)} h_B(t, t - \tau)x_B(\tau)d\tau + w_B(t), \quad (41)$$

where $\tau_{\min}(t) = \max\{0, t - T_d\}$, $\tau_{\max}(t) = \min\{t, T_c\}$, T_d denotes the maximum delay spread of the propagation channel and $w_B(t)$ is the complex valued noise in the baseband. Here, we made use of the fact that $h_B(t, \tau) = 0$ for $\tau < 0$ (due to

causality) and $\tau > T_d$, and $x_B(\tau) = 0$ for $\tau > T_c$, to arrive at the upper and lower limits of the integral in (41). Using (3), (40) and (41), the in-phase and quadrature components of the received signal can be expressed in the form:

$$y_{B,\text{Re}}(t) = \sum_{k=0}^{N-1} H_{k,\text{Re}}^{\text{Re}}(t)s_{k,\text{Re}} + H_{k,\text{Re}}^{\text{Im}}(t)s_{k,\text{Im}} + w_{B,\text{Re}}(t), \quad (42)$$

$$y_{B,\text{Im}}(t) = \sum_{k=0}^{N-1} H_{k,\text{Im}}^{\text{Re}}(t)s_{k,\text{Re}} + H_{k,\text{Im}}^{\text{Im}}(t)s_{k,\text{Im}} + w_{B,\text{Im}}(t), \quad (43)$$

where,

$$H_{k,\text{Re}}^{\text{Re}}(t) = \int_{\tau_{\min}^{(k)}(t)}^{\tau_{\max}^{(k)}(t)} h_{B,\text{Re}}(t, t - \tau)g(\tau - kT) \cos \phi_B(\tau)d\tau - \int_{\tau_{\min}^{(k)}(t)}^{\tau_{\max}^{(k)}(t)} h_{B,\text{Im}}(t, t - \tau)g(\tau - kT) \sin \phi_B(\tau)d\tau, \quad (44)$$

$$H_{k,\text{Re}}^{\text{Im}}(t) = - \int_{\tau_{\min}^{(k)}(t)}^{\tau_{\max}^{(k)}(t)} h_{B,\text{Re}}(t, t - \tau)g(\tau - kT) \sin \phi_B(\tau)d\tau - \int_{\tau_{\min}^{(k)}(t)}^{\tau_{\max}^{(k)}(t)} h_{B,\text{Im}}(t, t - \tau)g(\tau - kT) \cos \phi_B(\tau)d\tau, \quad (45)$$

$$H_{k,\text{Im}}^{\text{Re}}(t) = \int_{\tau_{\min}^{(k)}(t)}^{\tau_{\max}^{(k)}(t)} h_{B,\text{Re}}(t, t - \tau)g(\tau - kT) \sin \phi_B(\tau)d\tau + \int_{\tau_{\min}^{(k)}(t)}^{\tau_{\max}^{(k)}(t)} h_{B,\text{Im}}(t, t - \tau)g(\tau - kT) \cos \phi_B(\tau)d\tau, \quad (46)$$

$$H_{k,\text{Im}}^{\text{Im}}(t) = \int_{\tau_{\min}^{(k)}(t)}^{\tau_{\max}^{(k)}(t)} h_{B,\text{Re}}(t, t - \tau)g(\tau - kT) \cos \phi_B(\tau)d\tau - \int_{\tau_{\min}^{(k)}(t)}^{\tau_{\max}^{(k)}(t)} h_{B,\text{Im}}(t, t - \tau)g(\tau - kT) \sin \phi_B(\tau)d\tau, \quad (47)$$

$\phi_B(t) = 2\pi(f_L t_r(t) + m_c t_r^2(t) - f_c t)$, $\tau_{\min}^{(k)}(t) = \max\{0, t - T_d, kT\}$, $\tau_{\max}^{(k)}(t) = \min\{t, T_c, (k+1)T\}$, $w_{B,\text{Re}}(t)$ and $w_{B,\text{Im}}(t)$ are the real valued additive noises in the in-phase and quadrature channels. After sampling along t and τ axes, the received signal samples from (42)-(43) can be stacked and expressed in the form of (9). Entries of the channel matrix, $H \in \mathbb{R}^{NL \times 2N}$, are found from discretized versions of (44)-(47). At time $t = nT_s$, the in-phase and quadrature measurement samples are given by

$$\mathbf{y}_B[n] = \sum_{k=0}^{N-1} H_{n,k} \mathbf{s}_k + \mathbf{w}_B[n], \quad (48)$$

where $\mathbf{y}_B[n] = [y_{B,\text{Re}}(nT_s), y_{B,\text{Im}}(nT_s)]^T$, $H_{n,k} \in \mathbb{R}^{2 \times 2}$ is the block matrix,

$$H_{n,k} = \begin{bmatrix} H_{k,\text{Re}}^{\text{Re}}(nT_s) & H_{k,\text{Re}}^{\text{Im}}(nT_s) \\ H_{k,\text{Im}}^{\text{Re}}(nT_s) & H_{k,\text{Im}}^{\text{Im}}(nT_s) \end{bmatrix} \in \mathbb{R}^{2 \times 2}, \quad (49)$$

TABLE III
S2C PARAMETERS USED IN SEC. VI-C

Frequency band ($f_L - f_H$)	10 - 18 kHz
Chirp rate ($2m_c$)	800 kHz/s
Symbol duration (T)	0.5 ms
Sweep duration (T_{sw})	10 ms
Guard interval (T_g)	25 ms

The channel matrix, G_B , after gradient heterodyne and lowpass filtering is given by

$$G_B = Q_B^T H \in \mathbb{R}^{2N \times 2N}, \quad (50)$$

where $Q_B = \text{diag}\{Q_{B,0}, Q_{B,1}, \dots, Q_{B,N-1}\} \in \mathbb{R}^{2NL \times 2N}$,

$$Q_{B,k} = \text{diag}(\tilde{\mathbf{g}}) \begin{bmatrix} R_{\phi_B^{(k)}}[0] + R_{\phi_B^{(k)}}[0] - \frac{\pi}{2} \\ R_{\phi_B^{(k)}}[1] + R_{\phi_B^{(k)}}[1] - \frac{\pi}{2} \\ \vdots \\ R_{\phi_B^{(k)}}[L-1] + R_{\phi_B^{(k)}}[L-1] - \frac{\pi}{2} \end{bmatrix} \in \mathbb{R}^{2L \times 2},$$

R_θ is the rotation matrix,

$$R_\theta = \begin{bmatrix} \cos \theta & -\sin \theta \\ \sin \theta & \cos \theta \end{bmatrix} \in \mathbb{R}^{2 \times 2},$$

$\tilde{\mathbf{g}} = [g[0], g[0], g[1], g[1], \dots, g[L-1], g[L-1]]^T \in \mathbb{R}^{2L \times 1}$ and $\phi_B^{(k)}[l] = \phi_B \left((\tilde{k} - 1)T + lT_s \right)$, $\tilde{k} = k - \lfloor \frac{k}{M} \rfloor M$, $l = 0, \dots, L-1$.

Performance Evaluation: We now consider the performance of the proposed VSSD receiver over the WATERMARK channels for the S2C system in Table III. The channel datasets NOF1 and NCS1 in WATERMARK have a delay (τ) coverage of $T_d = 128$ ms and $T_d = 32$ ms respectively. Therefore, the measured impulse response of NOF1 (NCS1) channel is available only at an interval of $\Delta t = 128$ ms ($\Delta t = 32$ ms) along the t -axis. To compute the entries of the channel matrix, H and hence G , we require the channel impulse response at finer intervals corresponding to the baseband sampling frequency $F_s = 16$ kHz used in WATERMARK. We linearly interpolate the samples of measured baseband channel impulse response to obtain the response at finer intervals.

For timing and synchronization, a chirp pulse of duration $T_p = 20$ ms in the frequency band 10-18 kHz, called preamble, is prefixed to the transmission waveform. A guard interval of $T_g = 25$ ms is inserted between the preamble and the start of modulated waveform to avoid interference. Note that, although the delay coverage of NOF1 channel is $T_d = 128$ ms, the channel power delay profile falls by more than 20 dB beyond $T_g = 25$ ms. Matched filtering with the preamble waveform is used for detecting the start of the received waveform.

Figure 12 shows the computed channel matrix, G_B , for the first few bits in a received packet at one of the instances in the WATERMARK channel record NOF1. Significant ISI remains even after gradient heterodyne and lowpass filtering, as indicated by the strong off-diagonal entries in matrix G_B .

Figure 13 shows the performance of VSSD and MMSE receivers on the WATERMARK channel NOF1. NOF1 is a stable channel with coherence time spanning over several seconds. VSSD outperforms MMSE receiver by a margin

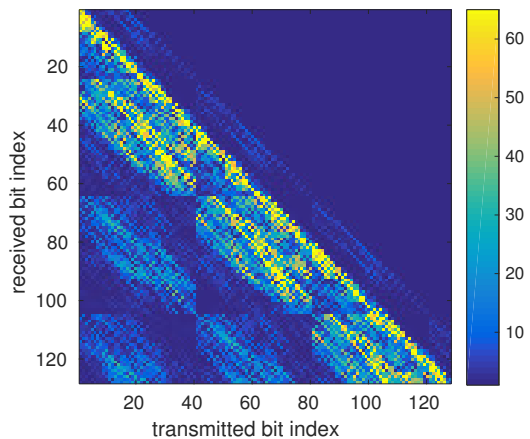


Fig. 12. Channel matrix after GradH processing at an instance in the WATERMARK channel record NOF1.

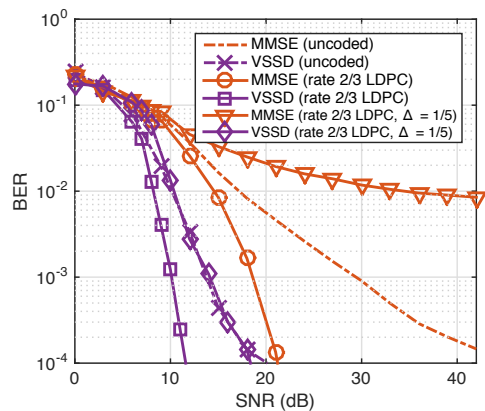


Fig. 13. BER of VSSD and MMSE receivers for S2C communications over the NOF1 channel in WATERMARK.

comparable to that in simulated UWA channels for both coded and uncoded communications in this real world channel also.

Figure 14 shows the BER of the proposed receiver on the NCS1 channel. NCS1 is characterized by a larger Doppler spread and therefore its impulse response varies significantly faster than NOF1. Both receivers require a higher SNR to achieve the same BER in NOF1 than NCS1. However, the strong relative performance of the VSSD receiver is maintained for both coded and uncoded communications even in this harsher UWA channel. While both NOF1 and NCS1 channels exhibit a comparable power delay profile, the coherence time of NCS1 is only about a tenth of a second that makes the channel prone to estimation errors. We see that, even in such challenging channel conditions as NCS1, VSSD is relatively resilient to channel estimation errors.

VII. CONCLUSIONS

In this work, we considered data symbol detection in an S2C receiver for doubly spread UWA channels. We formulated the problem of data detection for S2C communications over a wideband delay-scale channel and showed that the two existing S2C receivers are near MMSE decoders in only certain benign UWA channels. In more severe channels, where the existing

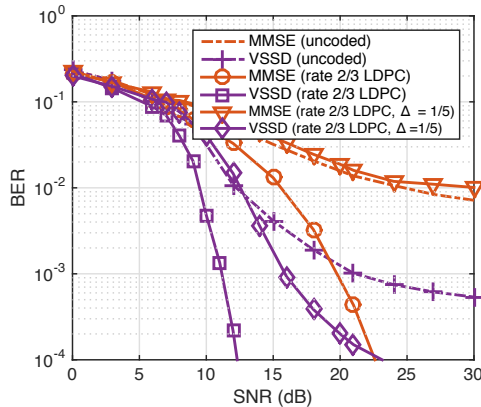


Fig. 14. BER of VSSD and MMSE receivers for S2C communications over the NCS1 channel in WATERMARK.

receivers either completely fail or must compromise on the data rate, we developed a new soft symbol decoder based on variational Bayes' inference. The input to the new decoder is the reduced data measurements at the output of the gradient heterodyne preprocessor of the existing S2C receivers.

Our proposed VSSD decoder estimates a probability vector (soft symbols) whose KL-distance to the true posterior of the symbol vector is minimized by iterating through a fixed point equation. In benign UWA channels, the VSSD decoder reduces to the existing S2C receivers. We showed that the fixed point iterations converge to a stationary point of the evidence lower bound in variational inference. We presented a few sufficient conditions that help to characterize the stationary point as a global maximum, local maximum or saddle point. Simulation results showed that VSSD significantly outperforms the MMSE decoder and maintains a robust performance, even under channel estimation errors, in challenging UWA channels. We applied the VSSD decoder on two contrasting real world UWA channels in the publicly available WATERMARK datasets. The new decoder outperforms the MMSE decoder in these channels as well, by a margin comparable to that in simulated UWA channels.

The ideal PAPR and low probability of intercept properties of S2C communications make it a promising candidate for terrestrial radio-frequency (RF) communications as well. Also, the VSSD algorithm developed in this paper is potentially applicable to other prevalent and emerging wireless communication systems.

APPENDIX

Evidence Lower Bound (ELBO): We derive the ELBO for soft symbol estimation. The first term in (23) is given by

$$\mathbb{E}_{q_\phi(\mathbf{s}|G, \mathbf{z})} \log p_\theta(\mathbf{z}|G, \mathbf{s}) = -N \log(2\pi\sigma^2) - \mathbb{E}_{q_\phi(\mathbf{s}|G, \mathbf{z})} \left[\frac{\|\mathbf{z} - G\mathbf{s}\|^2}{2\sigma^2} \right]. \quad (51)$$

Expanding the last term in (51), we get

$$\mathbb{E}_{q_\phi(\mathbf{s}|G, \mathbf{z})} [\|\mathbf{z} - G\mathbf{s}\|^2] = \|\mathbf{z}\|^2 - 2\mathbf{z}^T G \mathbb{E}_{q_\phi(\mathbf{s}|G, \mathbf{z})} [\mathbf{s}] + \mathbb{E}_{q_\phi(\mathbf{s}|G, \mathbf{z})} [\|G\mathbf{s}\|^2]. \quad (52)$$

We define:

$$q_{k, \text{Re}} \triangleq q_\phi \left(s_{k, \text{Re}} = \frac{1}{\sqrt{2}} \middle| G, \mathbf{z} \right) \in [0, 1], \quad (53)$$

$$q_{k, \text{Im}} \triangleq q_\phi \left(s_{k, \text{Im}} = \frac{1}{\sqrt{2}} \middle| G, \mathbf{z} \right) \in [0, 1]. \quad (54)$$

Note that the approximate posterior is completely specified by the soft symbol vector $\mathbf{q} \in \mathbb{R}^{2N}$ formed by stacking up $\mathbf{q}_k = [q_{k, \text{Re}}, q_{k, \text{Im}}]^T \in \mathbb{R}^2, k = 0, 1, \dots, N-1$. For our problem, we let the parameter $\phi \triangleq \mathbf{q}$.

The expectations in (52) can be evaluated as follows:

$$\mathbb{E}_{q_\phi(\mathbf{s}|G, \mathbf{z})} [s_{k, \text{Re}}] = \frac{1}{\sqrt{2}} (2q_{k, \text{Re}} - 1), \quad (55)$$

$$\mathbb{E}_{q_\phi(\mathbf{s}|G, \mathbf{z})} [s_{k, \text{Im}}] = \frac{1}{\sqrt{2}} (2q_{k, \text{Im}} - 1), \quad (56)$$

$$\mathbb{E}_{q_\phi(\mathbf{s}|G, \mathbf{z})} [\|G\mathbf{s}\|^2] = \sum_{l=0}^{2N-1} \mathbb{E}_{q_\phi(\mathbf{s}|G, \mathbf{z})} [G\mathbf{s}]_l^2, \quad (57)$$

$$\mathbb{E}_{q_\phi(\mathbf{s}|G, \mathbf{z})} [G\mathbf{s}]_l^2 = \sum_{k=0}^{N-1} \left(\eta_{l, k} + \nu_{l, k} \sum_{m \neq k} \nu_{l, m} \right), \quad (58)$$

where

$$\eta_{l, k} = \frac{1}{2} G_{l, k, \text{Re}}^2 + \frac{1}{2} G_{l, k, \text{Im}}^2 + G_{l, k, \text{Re}} G_{l, k, \text{Im}} (2q_{k, \text{Re}} - 1) (2q_{k, \text{Im}} - 1), \quad (59)$$

$$\nu_{l, m} = \frac{1}{\sqrt{2}} G_{l, m, \text{Re}} (2q_{m, \text{Re}} - 1) + \frac{1}{\sqrt{2}} G_{l, m, \text{Im}} (2q_{m, \text{Im}} - 1). \quad (60)$$

The ELBO regularizing term in (23) is

$$\mathbb{E}_{q_\phi(\mathbf{s}|G, \mathbf{z})} \left[\log \frac{q_\phi(\mathbf{s}|G, \mathbf{z})}{p_\theta(\mathbf{s})} \right] = KL(q_\phi \| p_\theta). \quad (61)$$

We assume a uniform prior $p_\theta(\mathbf{s}) = \frac{1}{2^{2N}}$. We have:

$$\mathbb{E}_{q_\phi(\mathbf{s}|G, \mathbf{z})} \left[\log \frac{q_\phi(\mathbf{s}|G, \mathbf{z})}{p_\theta(\mathbf{s})} \right] = \log 2^{2N} - \sum_{k=0}^{N-1} [\mathcal{H}(q_{k, \text{Re}}) + \mathcal{H}(q_{k, \text{Im}})], \quad (62)$$

where \mathcal{H} is the binary entropy function given by

$$\mathcal{H}(q) = -q \log q - (1 - q) \log(1 - q). \quad (63)$$

On combining the likelihood and regularization terms, we find the overall ELBO to be

$$\begin{aligned} \mathcal{L}(\theta, \mathbf{q}, \mathbf{z}) = & -N \log(2\pi\sigma^2) - \frac{\|\mathbf{z}\|^2}{2\sigma^2} + \frac{1}{\sqrt{2}\sigma^2} \mathbf{z}^T G(2\mathbf{q} - 1) \\ & - \frac{1}{2\sigma^2} \sum_{l=0}^{2N-1} \sum_{k=0}^{N-1} \left(\eta_{l, k} + \nu_{l, k} \sum_{m \neq k} \nu_{l, m} \right) - \log 2^{2N} \\ & + \sum_{k=0}^{N-1} -q_{k, \text{Re}} \log q_{k, \text{Re}} - (1 - q_{k, \text{Re}}) \log(1 - q_{k, \text{Re}}) \\ & + \sum_{k=0}^{N-1} -q_{k, \text{Im}} \log q_{k, \text{Im}} - (1 - q_{k, \text{Im}}) \log(1 - q_{k, \text{Im}}). \quad (64) \end{aligned}$$

Known Noise Variance: In this case, we take θ to be the empty set. The derivative of the overall cost function with respect to $q_{k^*,\text{Re}}$ is given by

$$\begin{aligned} \frac{\partial \mathcal{L}}{\partial q_{k^*,\text{Re}}} &= \frac{\sqrt{2}}{\sigma^2} \mathbf{z}^T G_{:,k^*,\text{Re}} \\ &- \frac{1}{2\sigma^2} \sum_{l=0}^{2N-1} \left(\frac{\partial \eta_{l,k^*}}{\partial q_{k^*,\text{Re}}} + 2 \frac{\partial \nu_{l,k^*}}{\partial q_{k^*,\text{Re}}} \sum_{m \neq k^*} \nu_{l,m} \right) \\ &- \log q_{k^*,\text{Re}} + \log(1 - q_{k^*,\text{Re}}). \end{aligned} \quad (65)$$

We have $\frac{\partial \eta_{l,k^*}}{\partial q_{k^*,\text{Re}}} = 2G_{l,k^*,\text{Re}}G_{l,k^*,\text{Im}}(2q_{k^*,\text{Im}} - 1)$ and $\frac{\partial \nu_{l,k^*}}{\partial q_{k^*,\text{Re}}} = \sqrt{2}G_{l,k^*,\text{Re}}$. The above can be simplified to

$$\frac{\partial \mathcal{L}}{\partial q_{k^*,\text{Re}}} = \alpha_{k^*,\text{Re}} - \log q_{k^*,\text{Re}} + \log(1 - q_{k^*,\text{Re}}), \quad (66)$$

where

$$\begin{aligned} \alpha_{k^*,\text{Re}} &= \frac{\sqrt{2}}{\sigma^2} \mathbf{z}^T G_{:,k^*,\text{Re}} \\ &- \frac{1}{\sigma^2} \sum_{l=0}^{2N-1} G_{l,k^*,\text{Re}}G_{l,k^*,\text{Im}}(2q_{k^*,\text{Im}} - 1) \\ &- \frac{\sqrt{2}}{\sigma^2} \sum_{l=0}^{2N-1} G_{l,k^*,\text{Re}} \sum_{m \neq k^*} \nu_{l,m}. \end{aligned} \quad (67)$$

Setting $\frac{\partial \mathcal{L}}{\partial q_{k^*,\text{Re}}} = 0$, we get $q_{k^*,\text{Re}} = \varphi(\alpha_{k^*,\text{Re}})$, where $\varphi(x) = \frac{1}{1+e^{-x}}$. Similarly, setting $\frac{\partial \mathcal{L}}{\partial q_{k^*,\text{Im}}} = 0$, we get $q_{k^*,\text{Im}} = \varphi(\alpha_{k^*,\text{Im}})$ where

$$\begin{aligned} \alpha_{k^*,\text{Im}} &= \frac{\sqrt{2}}{\sigma^2} \mathbf{z}^T G_{:,k^*,\text{Im}} \\ &- \frac{1}{\sigma^2} \sum_{l=0}^{2N-1} G_{l,k^*,\text{Im}}G_{l,k^*,\text{Re}}(2q_{k^*,\text{Re}} - 1) \\ &- \frac{\sqrt{2}}{\sigma^2} \sum_{l=0}^{2N-1} G_{l,k^*,\text{Im}} \sum_{m \neq k^*} \nu_{l,m}. \end{aligned} \quad (68)$$

Stacking up $\mathbf{q}_k = [q_{k^*,\text{Re}}, q_{k^*,\text{Im}}]^T \in \mathbb{R}^2$ into a vector, we get the following fixed point equations:

$$\mathbf{q} = \varphi(\boldsymbol{\alpha}), \quad (69)$$

where the vector $\boldsymbol{\alpha} \in \mathbb{R}^{2N}$ is formed by stacking $\boldsymbol{\alpha}_k = [\alpha_{k^*,\text{Re}}, \alpha_{k^*,\text{Im}}]^T \in \mathbb{R}^2, k = 0, 1, \dots, N-1$.

Unknown Noise Variance: In this case, we take $\theta = \{\sigma^2\}$. Differentiating the ELBO in (64) with respect to σ^2 , we get

$$\begin{aligned} \frac{\partial \mathcal{L}}{\partial \sigma^2} &= -\frac{N}{\sigma^2} + \frac{\|\mathbf{z}\|^2}{2\sigma^4} - \frac{1}{\sqrt{2}\sigma^4} \mathbf{z}^T G(2\mathbf{q} - 1) \\ &+ \frac{1}{2\sigma^4} \sum_{l=0}^{2N-1} \sum_{k=0}^{N-1} \left(\eta_{l,k} + \nu_{l,k} \sum_{m \neq k} \nu_{l,m} \right). \end{aligned} \quad (70)$$

Setting $\frac{\partial \mathcal{L}}{\partial \sigma^2} = 0$ and solving for σ^2 , we find

$$\begin{aligned} \hat{\sigma}^2 &= \frac{\|\mathbf{z}\|^2}{2N} - \frac{1}{\sqrt{2}N} \mathbf{z}^T G(2\mathbf{q} - 1) \\ &+ \frac{1}{2N} \sum_{l=0}^{2N-1} \sum_{k=0}^{N-1} \left(\eta_{l,k} + \nu_{l,k} \sum_{m \neq k} \nu_{l,m} \right). \end{aligned} \quad (71)$$

Unknown Channel and Noise Variance: In this case, we take $\theta = \{\sigma^2, G\}$. To differentiate the ELBO with respect to G , we notice that the terms in (64) that depend on G come from the left hand side of (52), i.e.,

$$\mathcal{L}_G = \mathbb{E}_{q_{\phi(\mathbf{s}|G,\mathbf{z})}} \left[(\mathbf{z} - G\mathbf{s})^T (\mathbf{z} - G\mathbf{s}) \right]. \quad (72)$$

On differentiating \mathcal{L}_G with respect to $G_{i,j}$ and setting to zero we get the following system of equations:

$$G\bar{\mathbf{s}} = \mathbf{z}, \quad (73)$$

where $\bar{\mathbf{s}} \triangleq \mathbb{E}_{q_{\phi(\mathbf{s}|G,\mathbf{z})}} [\mathbf{s}]$. The j th entry of $\bar{\mathbf{s}}$ is given by $\bar{s}_j = \frac{1}{\sqrt{2}}(2q_j - 1)$, if a data symbol is mounted at j th symbol location. At locations where the pilot symbols are mounted (to facilitate channel estimation), we have $\bar{s}_j = p_j$, where p_j is a known pilot symbol mounted at j th location. The channel matrix estimate can be refined using (73) once an initial estimate of the soft symbol vector is obtained through the fixed point update in (69). Note that G has $4N^2$ entries that need to be estimated from $2N$ equations in (73). One way to accomplish this is to exploit channel sparsity as in [21]. To see that, we make use of the relation $G = Q^T H$ and rewrite (73) in the form:

$$A\mathbf{h} = \mathbf{z}, \quad (74)$$

where $A = \sum_{i=0}^{N-1} (\bar{s}_{2i} Q^T C_i - \bar{s}_{2i+1} Q^T S_i) \in \mathbb{R}^{2N \times N_p}$. Now, following the approach in [21], equation (74) can be readily turned into a form suitable for estimating the channel parameters $\{h_p, \tilde{\tau}_p, b_p : p = 0, 1, \dots, N_p - 1\}$. The expression for the noise variance is the same as in (71), and is evaluated during the iterations once the soft symbol vector and the channel estimates are obtained using the fixed point update and (73), respectively.

REFERENCES

- [1] K. P. Arunkumar and C. R. Murthy, "Variational soft symbol decoding for sweep spread carrier based underwater acoustic communications," in *IEEE 20th International Workshop on Signal Processing Advances in Wireless Communications*, Cannes, France, Jul. 2019.
- [2] F. Campagnaro, R. Francescon, P. Casari, R. Diamant, and M. Zorzi, "Multimodal underwater networks: Recent advances and a look ahead," in *WUWNet 2017, Halifax, Canada*, Nov. 2019.
- [3] Y. Li, Y. Zhang, W. Li, and T. Jiang, "Marine wireless big data: Efficient transmission, related applications, and challenges," *IEEE Trans. Wireless Commun.*, vol. 25, no. 1, pp. 19–25, Feb. 2018.
- [4] Y. Li, S. Wang, C. Jin, Y. Zhang, and T. Jiang, "A survey of underwater magnetic induction communications: Fundamental issues, recent advances, and challenges," *IEEE Commun. Surveys Tuts.*, vol. 21, no. 3, pp. 2466–2487, third quarter 2019.
- [5] M. Stojanovic and J. Preisig, "Underwater acoustic communication channels: Propagation models and statistical characterization," *IEEE Commun. Mag.*, vol. 47, no. 1, pp. 84–89, Jan. 2009.
- [6] K. G. Kebkal and R. Bannasch, "Sweep-spread carrier for underwater communication over acoustic channels with strong multipath propagation," *J. Acoust. Soc. Am.*, vol. 112, no. 5, pp. 2043–2052, Nov. 2002.
- [7] Evologics GmbH, Ackerstrasse 76, 13355 Berlin, Germany. [Online]. Available: <https://evologics.de/acoustic-modems>
- [8] "Underwater acoustic MODEMS," in *Product Information Guide*. Evologics GmbH.
- [9] D. Robb, J. Willners, N. Valeyrie, F. Garcia, A. Laskov, X. Liu, P. Patron, H. Hastie, and Y. Petillot, "A natural language interface with relayed acoustic communications for improved command and control of AUVs," in *2018 IEEE/OES Autonomous Underwater Vehicle Workshop (AUV)*. IEEE, Nov. 2018.

- [10] A. Signori, F. Campagnaro, F. Steinmetz, B.-C. Renner, and M. Zorzi, "Data gathering from a multimodal dense underwater acoustic sensor network deployed in shallow fresh water scenarios," *Journal of Sensor and Actuator Networks*, vol. 8, no. 55, Nov. 2019.
- [11] D. Carlson, A. Ostrovskii, K. Kebkal, and H. Gildor, *Moored automatic mobile profilers and their application*. LAP LAMBERT Academic Publishing, June 2013, pp. 169–206.
- [12] K. G. Kebkal and R. Bannasch, "Method and devices for transmitting and receiving information," *U.S. Patent*, vol. 6,985,749 B2, Jan. 2006.
- [13] K. Kebkal, A. K. Kebkal, and G. A. Ermolin, "Mathematic and experimental evaluation of phase errors when receiving hydro-acoustic PSK-signals with sweep-spread carrier in reverberant underwater environments," in *Proc. MTS/IEEE OCEANS Conf.*, June 2013.
- [14] K. G. Kebkal, O. G. Kebkal, and R. Bannasch, "Synchronisation of underwater communication receivers by means of swept pulses," in *Proc. of the 4th Int. Conf. on Underwater Acou. Measurements: Technologies and Results*, June 2011.
- [15] K. G. Kebkal, V. K. Kebkal, O. G. Kebkal, and R. Petroccia, "Clock synchronization in underwater acoustic networks during payload data exchange," in *Proc. 2nd Int. Conf. Exhibit. Underwater Acoust.*, June 2014.
- [16] K. Kebkal, A. Kebkal, and V. Kebkal, "Synchronization tools of acoustic communication devices in control of underwater sensors, distributed antennas, autonomous underwater vehicles," in *Gyroscopy and Navigation*, vol. 5, no. 4. Pleiades Publishing, 2014, pp. 257–265.
- [17] L. Marchetti and R. Reggiannini, "An efficient receiver structure for sweep-spread-carrier underwater acoustic links," *IEEE J. of Ocean. Eng.*, vol. 41, no. 2, pp. 440–449, April 2016.
- [18] Y. Jiang and P. Antonia, "Discrete time-scale characterization of wideband time-varying systems," *IEEE Trans. Signal Process.*, vol. 54, no. 4, pp. 1364–1375, April 2006.
- [19] H. Franz and M. Gerald, *Wireless Communications Over Rapidly Time-Varying Channels*. Burlington, MA 01803, USA: Elsevier, 2011.
- [20] X. Jiang, W.-J. Zeng, and X.-L. Li, "Time delay and Doppler estimation for wideband acoustic signals in multipath environments," *J. Acoust. Soc. Am.*, vol. 130, no. 2, pp. 850–857, Aug. 2011.
- [21] C. R. Berger, S. Zhou, J. C. Preisig, and P. Willett, "Sparse channel estimation for multicarrier underwater acoustic communication: From subspace methods to compressed sensing," *IEEE Trans. Signal Process.*, vol. 57, no. 5, pp. 2941–2965, May 2011.
- [22] J. Z. Huang, S. Zhou, J. Huang, C. R. Berger, and P. Willett, "Progressive inter-carrier interference equalization for OFDM transmission over time-varying underwater acoustic channels," *IEEE J. Sel. Topics Signal Process.*, vol. 5, no. 8, pp. 1524–1536, Dec. 2011.
- [23] S. Zhou and Z. Wang, "OFDM for underwater acoustic communications." Wiley, 2014.
- [24] M. Stojanovic and L. Freitag, "Multichannel detection for wideband underwater acoustic CDMA communications," *IEEE J. of Ocean. Eng.*, vol. 31, no. 3, pp. 685–695, Jul. 2006.
- [25] Z. Wang, S. Zhou, G. B. Giannakis, C. R. Berger, and J. Huang, "Frequency-domain oversampling for zero-padded OFDM in underwater acoustic communications," *IEEE J. of Ocean. Eng.*, vol. 37, no. 1, pp. 14–24, Jan. 2012.
- [26] A. Goldsmith, *Wireless Communications*. Cambridge University Press, 2005.
- [27] S. S. Thoota and C. R. Murthy, "Variational Bayesian inference based soft-symbol decoding for uplink massive MIMO systems with low resolution ADCs," in *Proc. Asilomar Conference on Signals, Systems and Computers*, Nov. 2019.
- [28] —, "Quantized variational Bayesian joint channel estimation and data detection for uplink massive MIMO systems with low resolution ADCs," in *Proc. IEEE International Workshop on Machine Learning for Signal Processing, Pittsburg, PA, USA*, Oct. 2019.
- [29] B. Li, S. Zhou, M. Stojanovic, L. Freitag, and P. Willett, "Multicarrier communication over underwater acoustic channels with nonuniform Doppler shifts," *IEEE J. Ocean. Eng.*, vol. 33, no. 2, pp. 1638–1649, Apr. 2008.
- [30] D. P. Kingma and M. Welling, "Auto-encoding variational Bayes," in *Proceedings of the 2nd International Conference on Learning Representations*, Apr. 2014.
- [31] C. Studer, M. Wenk, A. Burg, and H. Bölcskei, "Soft-output MIMO detection algorithms: Performance and implementation aspects," in *Proc. of the 40th Asilomar Conference on Signals, Systems, and Computers*, Oct. 2006.
- [32] C. Studer, A. Burg, and H. Bölcskei, "Soft-output sphere decoding: Algorithms and VLSI implementation," *IEEE J. Sel. Areas Commun.*, vol. 26, no. 2, pp. 290–300, Feb. 2008.
- [33] "MATLAB Communications System Toolbox, version 6.3," The Mathworks, Inc., Natick, Massachusetts.
- [34] M. Helmling, S. Scholl, F. Gensheimer, T. Dietz, K. Kraft, S. Ruzika, and N. Wehn, "Database of Channel Codes and ML Simulation Results," www.uni-kl.de/channel-codes, 2019.
- [35] P. Qarabaqi and M. Stojanovic, "Statistical characterization and computationally efficient modeling of a class of underwater acoustic communication channels," *IEEE J. Ocean. Eng.*, vol. 38, no. 4, pp. 701–717, Oct. 2012.
- [36] M. Stojanovic. Acoustic channel simulator. [Online]. Available: <http://millitsa.coe.neu.edu/?q=research/simulator>
- [37] P. A. van Walree, F. Socheleau, R. Otne, and T. Jensenud, "The Watermark benchmark for underwater acoustic modulation schemes," *IEEE J. Ocean. Eng.*, vol. 42, no. 4, pp. 1007–1018, Oct. 2017.
- [38] R. Otne, P. A. van Walree, and T. Jensenud, "Validation of replay-based underwater acoustic communication channel simulation," *IEEE J. Ocean. Eng.*, vol. 38, no. 4, pp. 689–700, Oct. 2013.
- [39] P. A. van Walree, R. Otne, and T. Jensenud, "The Watermark manual and users guide version 1.0," in *Norwegian Defense Research Establishment (FFI)*, Nov. 2016.



Arunkumar K. P. received the B. Tech. (Hons) degree in Electrical and Electronics Engineering, in 1998, from the Calicut University, India. Since 2000, he has been working as a Scientist at Naval Physical & Oceanographic Laboratory, Defence Research & Development Organization (DRDO), Kochi, India. He received the M. E. degree, in 2007, in Signal Processing, from the Indian Institute of Science (IISc), Bangalore, India, as a sponsored candidate from DRDO. He was awarded the Prof. I. S. N. Murthy medal for the best M. E. student in Signal Processing discipline at IISc, Bangalore, for the year 2005-2007. He is currently pursuing Ph. D. as an external registrant from DRDO at the Signal Processing for Communications Lab in the Department of Electrical Communication Engineering, IISc, Bangalore. His research interests include sparse signal recovery algorithms, sensor array signal processing and underwater acoustic communications.



Chandra R. Murthy (S'03–M'06–SM'11) received the B. Tech. degree in Electrical Engineering from the Indian Institute of Technology, Madras in 1998, the M. S. and Ph. D. degrees in Electrical and Computer Engineering from Purdue University and the University of California, San Diego, in 2000 and 2006, respectively. From 2000 to 2002, he worked as an engineer for Qualcomm Inc., where he worked on WCDMA baseband transceiver design and 802.11b baseband receivers. From Aug. 2006 to Aug. 2007, he worked as a staff engineer at Beceem Communications Inc. on advanced receiver architectures for the 802.16e Mobile WiMAX standard. In Sept. 2007, he joined the Department of Electrical Communication Engineering at the Indian Institute of Science, Bangalore, India, where he is currently working as a Professor.

His research interests are in the areas of energy harvesting communications, multiuser MIMO systems, and sparse signal recovery techniques applied to wireless communications. He has 50+ journal and 80+ conference papers to his credit. He is a recipient of the MeitY Young Faculty Fellowship from the Govt. of India and the Prof. Satish Dhawan state award for engineering from the Karnataka State Government. His paper won the best paper award in the Communications Track in the National Conference on Communications 2014. He was an associate editor for the IEEE Signal Processing Letters during 2012–16. He is a past Chair of the IEEE Signal Processing Society, Bangalore Chapter. He was an elected member of the IEEE SPCOM Technical Committee for the years 2014–16, and has been re-elected for the years 2017–19. He is serving as an associate editor for the IEEE Transactions on Signal Processing, the IEEE Transactions on Communications, and Sadhana Academy Proceedings in Engineering Sciences.